www.sciencemag.org/cgi/content/full/334/6061/1424/DC1

Supporting Online Material for

Explaining Seasonal Fluctuations of Measles in Niger Using Nighttime Lights Imagery

N. Bharti,* A. J. Tatem, M. J. Ferrari, R. F. Grais, A. Djibo, B. T. Grenfell

*To whom correspondence should be addressed. E-mail: nbharti@princeton.edu

Published 9 December 2011, *Science* **334**, 1424 (2011)
DOI: 10.1126/science.1210554

This PDF file includes

Supporting Online Material

Supporting Online Material Part 1: Data acquisition, processing, and analyses of spatial variation in brightness within cities

Introduction

Operational Linescan System (OLS) instruments onboard Defense Meteorological Satellite Program (DMSP) satellites can detect areas of anthropogenically derived light sources (electric lighting and fires), which indicate the presence of human settlements (*15, 16*). The spatial resolution of DMSP OLS imagery permits a spatial analysis of changes within cities, which is not possible by using estimated measles transmission rates. Long-term measles case reports in Niger are consistently available at the level of the health district, the spatially smallest of which is the entire city of Maradi (*28*). Here, we measure changes in brightness as a proxy for relative density within cities. The goal of this analysis is to estimate spatiotemporal changes of risk with respect to disease transmission within cities. We do this by using nighttime lights brightness to detect locations and times of highest density and greatest density fluctuations within cities. With the identification of such areas, intervention efforts can be planned with increased efficiency and precision.

This study focused on five cities: four from Niger and one from Nigeria: Niamey, Maradi, Zinder, Agadez, and Katsina (Fig. S1A). The nighttime lights brightness of Niamey, Maradi, and Zinder were analyzed because weekly measles incidence data from 1995–2004 were available for each of these cities (*2, 28*). In addition, the northern city of Agadez was included for contrast; seasonal rainfall and agriculture are minimal, and year-round employment in uranium mines in the region does not contribute to seasonal labor migration. Although long-term measles data were not available for the city of Agadez, long-term measles data from the larger district of Agadez showed far less pronounced seasonal increases in measles incidence than was seen in other districts, particularly those in the south (*2*). Finally, Katsina in Nigeria was included because previous work has shown that this area is likely to be an epidemiologically important component of the metapopulation that includes Maradi, Zinder, and surrounding health districts in southern Niger (*29*).

Methods

Cities and rainfall

Daily rainfall estimates were obtained from 2003 to 2006 from the National Oceanic and Atmospheric Administration's (NOAA) Climate Prediction Center's (CPC) Morphing Technique (CMORPH) (*30*) for all of Niger. The Ministry of Health estimated the population sizes and birth rates for the health districts in Niger for 2004 (*28*) and the population size of Katsina, Nigeria was taken from the 2006 census.

For each of the five urban areas described above, the urban and settlement polygon outlines were derived based on 2000 and 2005 Landsat imagery from either on-screen manual delineation or area-masked unsupervised per-pixel classifications sourced from the EarthSat—MDA GeoCover 2000 Stock (Landsat) scenes. The pixels included in the

maximum lighting extent were identified through the Global Rural Urban Mapping Project (GRUMP) urban extents data set, which was based principally on multiyear composite DMSP-OLS data (*22*). The DMSP-OLS data were used to identify stable lights for defining urban areas. No image thresholding was undertaken in the construction of the GRUMP urban extents dataset. As a result of the "overglow" effect associated with these images (*31*), mapped urban extents often extend beyond the true boundaries for larger cities. These extents were used to select appropriate images for nighttime lights analyses using the methods described below.

Nighttime lights and associated data

DMSP satellites orbit at low altitude (833 km) and provide visible and thermal-infrared images to visualize nighttime lights and detect cloud cover. The processed, georeferenced images, obtainable from the Space Physics Interactive Data Resource (SPIDR, http://spidr.ngdc.noaa.gov/spidr/), are available at ~1-km spatial resolution (0.00833 decimal degrees, resampled from the 2.7-km native resolution at the SPIDR). For most of the earth, a set of two images is captured twice a day, once during the daytime and once at night, between 7 p.m. and 11 p.m. One image is captured in the visible light spectrum and the other is a thermal infrared (TIR) image. The former enables detection of anthropogenically derived light sources, while the latter provides a method for detecting clouds in images (see below). To assess nighttime light brightness, DMSP-OLS images from the F15 satellite were used. We focused on the F15 satellite partly because it was operational during the time period when weekly measles case reports were available. The F15 OLS sensor was launched in 2000 and provided usable night lights images until 2008 (*32*).

Although images are taken daily, the vast majority are inappropriate for this method. Images must be thoroughly screened and selected carefully because many environmental elements can impact brightness measurements. First, lunar illumination can contaminate brightness measurements so images captured during bright moon phases were avoided. To ensure image comparability and minimize natural light contamination, images captured during times of low lunar illumination were selected using a lunar calendar. Moreover, to avoid solar contamination and reduce the impact of variability in human behavior, we only considered images that were captured between 7 p.m. and 10 p.m.

Cloud contamination can also affect brightness measurements. During preliminary analyses to identify candidate images, the SPIDR screened georeferenced images for cloud cover using an in-house constructed cloud algorithm for the pixels used in this study to eliminate images with cloud cover. The cloud algorithm compares the thermal band of the DMSP-OLS with surface temperature obtained from the NOAA—National Centers for Environmental Protection (NCEP) Global Forecast System (GFS) grids; areas that are significantly cooler than the surface temperature are deemed clouds. These preliminary analyses confirmed that the F15 satellite produced the most cloud-free, low lunar images during the period of interest. Based on the lunar cycles and cloud algorithm results, we then visually examined each TIR image thumbnail of all remaining candidate images. We selected images that were free of cloud cover over all pixels for all five cities of interest.

Images that met these initial screening requirements were acquired from the National Oceanic and Atmospheric Administration (NOAA) National Geophysical Data Center as georeferenced images. TIR values for all pixels within the urban extents of interest were extracted using R (*33*). TIR values are positively correlated with cloud presence so a conservative threshold was chosen, and images with TIR values over 50 [in their digital number (DN) format] were dropped from the analyses. For each of the remaining images that met all these requirements (n = 155), we extracted brightness values for each pixel of each city. For each image, the brightness value [also in the DN format, as was done in Agnew *et al*., 2008 (*17*)] was measured for each pixel within each defined urban extent. It is important to note that brightly lit areas can cause sensor saturation, whereas low-lit areas are undetectable (*34*) (see more below).

All the 155 images used were captured during 2000, 2002, 2003, and 2004. In order to create an annual signature of brightness, we arranged these images by calendar date (Fig. S1B). Because of satellite drift and gradual sensor degradation over time, the extracted brightness values were calibrated to ensure comparability between years. This was done using intercalibration equations, which were derived using overlapping nighttime brightness measurements during periods of two simultaneously operational satellites [detailed in Table 2 in Elvidge *et al*. 2009 (*32*)].

To detect city-wide patterns of *temporal* brightness fluctuations, we calculated the mean brightness value across all pixels within each city for each image. These brightness values were used for correlation against city-wide estimated transmission rates (Fig. 1F, main paper, and Fig. S2A). For visualization purposes, a cubic smoothing spline (df = 3) was fit to the relative brightness values; these are shown as smoothed curves for each city (Fig. 1E and Fig. S2B). To detect *spatial* variation in density fluctuations within cities, we calculated the mean and variance of individual pixel brightness measurements across all images (Fig. S2, C to E).

Results

The overall temporal patterns for seasonal changes in nighttime brightness for all five cities were qualitatively similar. Each city's brightness values fell below the mean during the rainy season and rose above the mean during the dry season, with the exception of Agadez, which had a later onset of consistent rain, by which time brightness values were below their mean annual value (Fig. S2, A and B). Compared with the other four cities in this analysis, the northern city of Agadez showed the least pronounced fluctuations in brightness (Table S1).

Spatially, all five cities contained pixels that were consistently brighter than the others. It was not surprising that these pixels were often located near the geographic city center (Fig. S2C). All five cities exhibit a positive correlation of varying strength between variance in pixel brightness and mean pixel brightness (correlation coefficients: Niamey = 0.33, $p < 0.01$; Maradi = 0.82, $p < 0.01$; Zinder = 0.67, $p < 0.01$; Agadez = 0.67, $p < 0.01$; Katsina = 0.58, $p < 0.01$). In the two largest cities, Niamey and Katsina, the correlation was weakest because this relationship turned over when the sensor became saturated and could no longer detect increased brightness (~64 here, Fig. S2D). Distance

from the city center was negatively correlated with mean pixel brightness and variance in brightness values (Fig. S2E). Exceptions to the latter relationship are seen in Niamey and Katsina, where pixels at the city center have low variance due to sensor saturation.

Discussion

Despite the difference in geographic size and total population size, similar patterns of spatial and temporal variation in brightness emerged in all five cities. The relatively lower fluctuations in brightness in Agadez are likely caused by comparatively fewer seasonal labor opportunities. Although agriculture cannot be heavily practiced this close to the desert and the brightness in Agadez fluctuates the least of all the cities, the brightness first falls below the mean at the onset of the rainy season in the southern, agricultural areas of Niger. This may reflect a small amount of long-distance seasonal agricultural relocation from this city, although measuring changes in brightness does not allow us to track individual movements or changes in the daily routines of nonmigrants.

It was not surprising that city centers were generally brightest, whereas increased distance from the city center was negatively correlated with mean brightness. The greatest fluctuation in brightness occurred either at the city center or very near the city center, in the case of pixel saturation at the city center.

Conclusion

Along with the seasonal signature of brightness fluctuations, the spatial patterns of brightness can highlight times and areas of greatest population density and greatest fluctuations in population density. Spatiotemporal patterns of population fluctuations are consistent across these five cities and this information can aid in planning intervention strategies.

Supporting Online Material Part 2: SEIR Model in Niamey

Introduction

To understand the impact of dynamic population density on the progression of a measles epidemic at high spatial and temporal resolution, we fit an explicit SEIR (Susceptible-Exposed-Infectious-Recovered) model to a measles outbreak from 2003 to 2004 with daily reported cases of measles each commune within the city of Niamey, Niger (*35*).

Methods

Brightness values

For the commune-level analysis of Niamey, brightness values were extracted for each pixel of each commune (pixels were assigned to a commune using the method described in supporting online material 1 for the city designation of pixels). For each image, the mean brightness value was taken across all pixels within a commune. A cubic smoothing spline (df = 3) was fit to the brightness values for each of the three communes independently across calendar dates (Fig. 2B). The resulting values were used to calculate

the derivative of the brightness curve for each commune, which was then used in the SEIR model (Fig. 2D and below).

Model

This approach measured the mechanism underlying the observed seasonally fluctuating incidence of disease. Previous models have incorporated seasonal fluctuations by fitting time-varying transmission parameters (β_t) and holding population density constant (*36*), despite proposing seasonal changes in population density as the underlying mechanism for the observed seasonal swings in disease incidence (*2*). This formulation had the implicit interpretation that contact rates were changing yet the population sizes in the model were held constant. Here we included changes in population size by explicitly including movements into and out of each settlement, as indexed by lights. Thus, we modify the basic SEIR model to include time-dependent migration (M_t) into and out of the susceptible (S) and exposed (E) class:

$$
\begin{aligned}
S_{t+1} &= S_t - \beta S_t \sum_{j=1}^{4} I_j + (M_{S,t}) \\
E^1_{t+1} &= E^1_t + \beta S_t \sum_{j=1}^{4} I_j - \phi E^1_t + (M_{E,t}) \\
E^2_{t+1} &= E^2_t + \phi E^1_t - \phi E^2_t \\
E^3_{t+1} &= E3 + \phi E^2_t - \phi E^3_t \\
I^1_{t+1} &= I^1_t + \phi E^3_t - \gamma I^1_t \\
I^2_{t+1} &= I^2_t + \gamma I^1_t - \gamma I^2_t \\
I^3_{t+1} &= I^3_t + \gamma I^2_t - \gamma I^3_t \\
I^4_{t+1} &= I^4_t + \gamma I^3_t - \gamma I^4_t \\
R_{t+1} &= R_t + \gamma I^4_t
\end{aligned}
\qquad \text{(Eq. 1)}
$$

In each commune, S_t, E_t, and I_t are the number of susceptible, exposed, and infectious individuals at time t, respectively, and β is a constant transmission parameter. Infected individuals progress through 3 stages in the exposed class and 4 stages in the infectious class to approximate gamma distributed durations in each of these classes (*9, 37*). The transitions through these stages occur at rate $\phi = 1/2$ and $\gamma = 1/2$ to give expected durations in the exposed and infectious classes of 6 and 8 days, respectively.

$M_{S,t}$ and $M_{E,t}$ represent the susceptible and infected individuals migrating in and out of the population of each commune in each time step. We modeled the migration into and out of the population as a linear function of the change in nighttime light brightness. Thus, the time-specific change in the susceptible and exposed classes are given by:

$$M_{S,t} = \Theta * P_S * \frac{dL}{dt}$$
$$M_{E,t} = \Theta * P_E * \frac{dL}{dt} \qquad \text{(Eq. 2)}$$

where Θ is the slope of the linear function and $\frac{dL}{dt}$ is the derivative of a smoothing spline fit to the nighttime lights brightness of each commune, The terms P_S and P_E are scaling constants that reflect the assumption that migrants should be disproportionately susceptible; we have presented the results from the ratio of P_S:P_E of 50:1in the main text, but the results from other ratios are discussed in detail below. At each daily time step, the number of individuals transitioning into and out of each class (S, E, I, R) was assumed to be a Poisson random variable with expectation equal to the values given in equations 1 and 2.

In Niamey in 2004, a 2-week vaccination campaign was conducted starting on day 161 of the measles epidemic. The campaign targeted all children 9–59 months of age with a goal of achieving 50% coverage. To incorporate the vaccination campaign, we assumed that the susceptible population was reduced by 50% over a 2-week period, using a constant daily rate, from day 161 to 175 of the epidemic.

Local health centers recorded daily measles cases presenting at clinics in each of the 3 communes in Niamey from calendar day 307 of 2003 through calendar day 172 of 2004. These case reports likely reflect an underestimate of the true number of measles cases. We model the reported cases on each day as a negative binomial random variable with mean equal to αI_t^1 and variance equal to σ. Thus, the cases presenting at clinics on any given day are only those transitioning from the exposed to infectious class on each day, when measles symptoms became apparent.

We fit the dynamic epidemic model (equations 1 and 2) to the reported daily measles cases for each commune using a Bayesian particle filter (*38*). The algorithm was as follows:

1. 50,000 draws for the parameters: β, migration rate (either Θ or nighttime lights-independent), S_0 (the initial susceptible population size), α, and σ from uniform prior distributions.
2. For each parameter draw from the prior, 5000 iterations of the stochastic epidemic model (equations 1 and 2) were run starting on epidemic day 1 (calendar day 307 of 2003) initialized with a single infected individual.
3. For each simulated trajectory, we evaluated the likelihood of observing the reported cases given the simulated incidence, I_t^1 under the negative binomial observation model.
4. The approximate likelihood for each draw from the prior was calculated as the average of the likelihoods for the 5000 simulated trajectories.
5. We then re-sampled the initial draws from the prior distribution, with replacement, with sampling weights equal to the approximate likelihood to arrive at a posterior distribution for the parameters.

We took the mean of the posterior distribution as a point estimate, and quantiles of the posterior distribution as interval estimates.

We further fit two additional models to each commune for the purposes of comparison. In the first we assumed no migration, i.e. we fixed Θ at 0. In the second, we fit a constant migration rate that was not informed by the pattern of nighttime lights. Both models were fit to each commune using the algorithm described above.

Sensitivity analysis of ratio of susceptible to infected migrants

We hypothesized that the timing of epidemics in Niamey was driven by a seasonal change in the density of susceptible hosts. Additionally, because measles was absent from Niamey prior to the 2003–04 outbreak, the infection was likely imported before the epidemic occurred. Bjørnstad *et al*. (*39*) have previously shown that immigration of infected individuals is important at the start of an epidemic, but has little impact on the trajectory of an epidemic once it is started. Individuals are infected with measles for only ~14 days, thus we presumed that, in any given time step, infected individuals should be rare relative to susceptible individuals among migrants. Because immunity is long-lasting, the majority of the population is immune or recovered (and therefore epidemiologically unimportant) (*39*); here we explored the sensitivity of our results to the ratio of susceptible to infected migrants. To do this, we fit the nighttime lights–informed model and the constant migration model across five different ratios of susceptible to infected individuals; 1:1, 10:1, 25:1, 50:1, and 100:1. (Note that the ratio of migrants is irrelevant in the model with no migration.) We compared the predicted number of days to reach the 10, 25, and 50% percentiles of total cases from simulated trajectories of the fitted models across all five ratios for all three models across all three communes (Fig. S3).

Although presented in Fig. S3, we note that the ratio of 1:1 is highly unlikely, as this would indicate that the proportion of the population of immigrants that was neither recovered nor immune was constantly equal parts susceptible and infected. In one interpretation, a susceptible to infected ratio of 1:1 would exceed the proportion of infected individuals observed at one time in this population, even during an epidemic, and would not be sustainable. Alternatively, this ratio could occur for a short time in a population that was almost entirely recovered, in which case epidemics would likely not occur.

Results

For each commune, the model simultaneously fit values for β, migration rate (either Θ or nighttime lights-independent), the initial susceptible population size (S_0), the observation rate, α, and the observation variance, σ. We found that for all communes, a model with seasonal migration, as indexed by nighttime lights brightness, predicted the timing and magnitude of reported measles cases far better than the other two models (Fig. 2D). The likelihood (approximated by the particle filter) for the nighttime lights–informed models was significantly greater than the competing models in all three communes (Table S2).

This was particularly apparent in communes 1 and 2, where the bulk of the cases occurred (Table S4).

Sensitivity analysis of ratio of susceptible to infected migrants

Under the nighttime lights–informed model, the time to each of the percentiles of cases was sensitive to the assumed ratio of susceptible to infected individuals, with earlier timing in commune 1 and 2 when infected individuals were rare among immigrants, and in commune 3 when infected individuals were common among immigrants. The nighttime lights–informed model replicated the timing of the 25% and 50% percentiles of cases in all three communes for settings in which infected immigrants were rare relative to susceptible immigrants. Under the constant migration model, the number of days to the percentiles was invariant to the assumed ratio.

The models with no migration and constant migration consistently underestimated the time to the percentiles of cases regardless of the assumed ratio. The nighttime lights–informed model tended to reproduce the observed time to the percentiles in all three communes for ratios at which infected migrants were relatively rare (i.e. susceptible to infected ratios greater than 10:1).

Both the nighttime lights–informed model and the model with no migration tended to produce trajectories in which the timing to the percentiles was ordered from commune 1 to 3; though there was considerable variation in the timing of percentiles in commune 3 when the ratio of susceptibles to infected migrants was low. Specifically, the model with no migration predicted the order of timings to 25 and 50% of cases to progress in order from commune 1 to 3.

Discussion

The model with no migration ($\Theta = 0$) and the model with constant migration both predicted the peak of the epidemic to be larger and occur earlier than observed. The model with constant migration estimated that the epidemic would take off immediately and progress rapidly.

The sensitivity analysis suggests that both the timing of epidemic percentiles compared to the observed epidemic and the relative ordering of percentiles in the three communes is relatively robust to the ratio of migrants while infected individuals are relatively rare within any given time step. For all analyses in the main text, we present results assuming that the ratio of susceptible to infected migrants is 50:1. While the cumulative number of infected individuals over the course of an epidemic may reach a large percentage of the susceptible pool, the short period of infection of only ~14 days indicates that infected individuals are likely to be relatively rare within the population at any given time point.

We note that commune 3 is the smallest of the three communes as measured by population size and numbers of measles cases. For these reasons, the model predictions from commune 3 are more sensitive to stochastic variation than either communes 1 or 2. This leads to variation across model trajectories, resulting in a wider range of predicted values than is seen for the other two communes (Fig. S3). Note that we are using the

shape of the brightness curves to estimates relative changes in incidence such that correctly predicting the timing of the onset and the peak of the epidemic using a stochastic model is more important than correctly predicting the magnitude of the epidemic, which is a simple scaling issue. The nighttime lights–informed model is able to predict the time to the percentiles of cases in all three communes. Although the predictions cover a wide range of values for the reasons mentioned above, the reported measles cases fall within the predicted boundaries from the nighttime lights–informed model.

The observed relatively late timing of the peak in nighttime brightness in commune 3 is interesting (Fig. 2B main paper). We do not currently have a clear explanation as to why the fluctuations of anthropogenic lights in this part of the city appeared to be out of phase with the rest of the city. The increase in brightness during the rainy season, however, definitively showed that the sensors are not affected by the rainy season and can detect increases in brightness year round. Commune 3 had the fewest cases and the timing of the intervention occurred when both cases and brightness were increasing. The reactive immunization campaign may have had a strong impact in commune 3, while it occurred after the peak of cases and brightness in communes 1 and 2.

Conclusion

Three explicit SEIR models fit to each of the three communes of Niamey showed that the estimated fluctuations in population size, based on changes in nighttime lights brightness, were necessary to explain the initial trajectory and overall magnitude of a measles epidemic in the city of Niamey during 2003–04. In all three communes, models that included nighttime lights brightness were also far more accurate in predicting the timing to percentiles of measles cases when compared to models that did not include nighttime lights; brightness. This approach could be beneficial for exploring the dynamics of directly transmitted diseases with possible density effects, such as waves of seasonal influenza (*40*) or emerging infections.

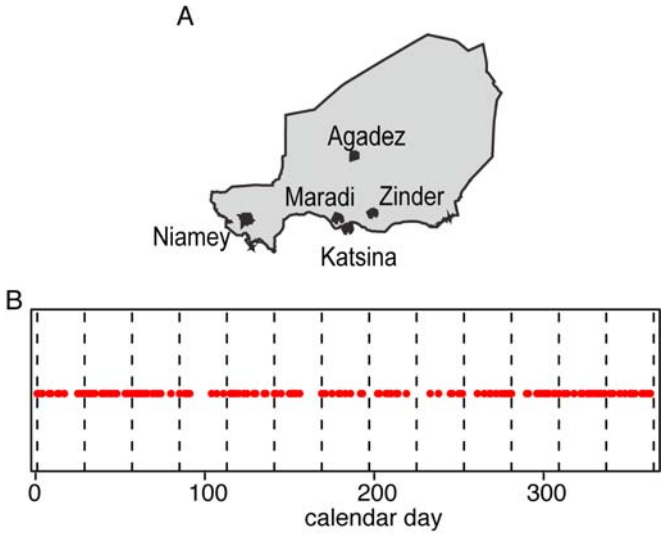

Figure S1. (**A**) Map showing locations of all five cities included in this study; four in Niger and one in Nigeria. (**B**) Red points indicate calendar dates of all images selected for this analysis. Dashed vertical lines delineate the two-week periods for which transmission rates were estimated (*I*).

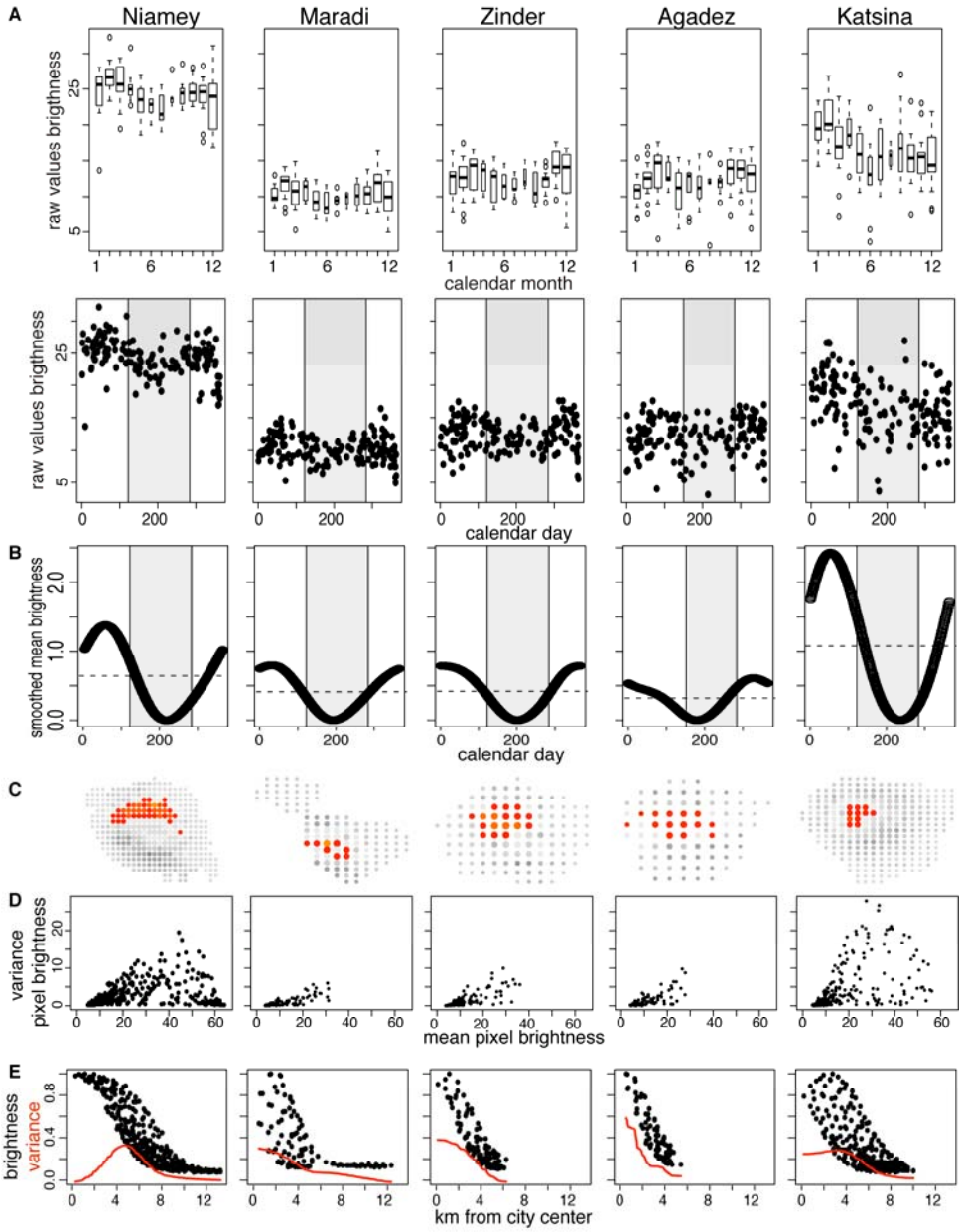

Figure S2. (**A**) Shaded gray area indicates duration of rainy season for each city. (Top) For all cities, raw brightness values from each image binned by month, from January to December. Each box indicates the interquartile range (box) and median (central line); whiskers extend to the nearest point less than 1.5 times the interquartile range.. Bottom: For all cities, raw brightness values by calendar day. (**B**) Smoothed (df = 3) relative brightness for each city plotted against calendar day from 1 to 365. Adjusted so minimum brightness is equal to zero for each city. Horizontal dashed line indicates mean brightness for each city. Shaded gray area indicates duration of rainy season for each city. (**C**) Map of pixels of each city included in this analysis. Color of pixel indicates relative mean brightness (orange = brightest; red = above mean; light grey = mean or slightly below; dark grey = below mean). (**D**) Variance in pixel brightness plotted against mean pixel brightness. This relationship turns over due to sensor saturation in the two largest cities included in this analysis, Niamey and Katsina. (**E**) Proportional mean pixel brightness (black points) and proportional pixel variance (red lines) plotted against distance from city center.

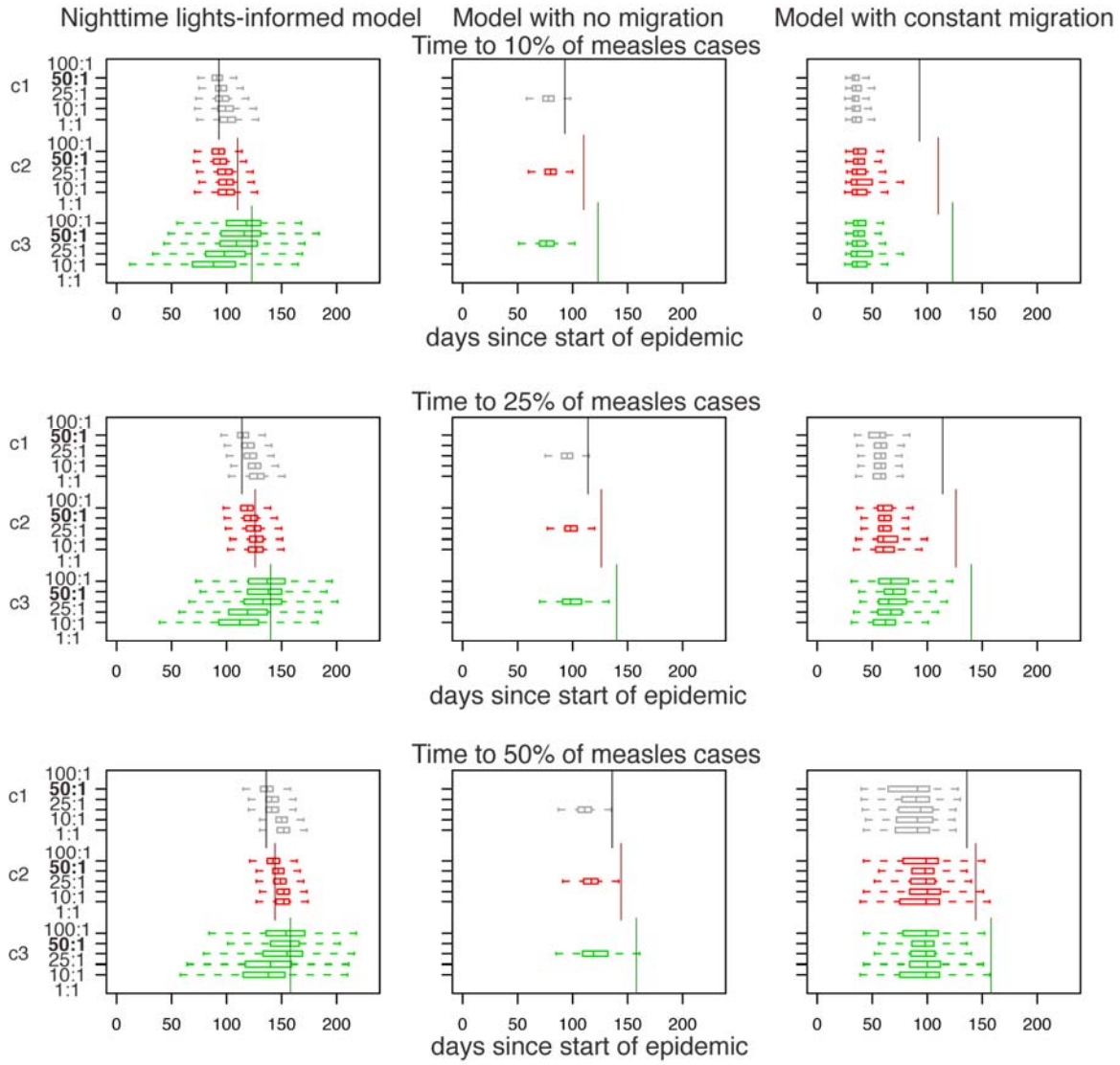

Figure S3. The sensitivity of the timing of outbreaks to the ratio of immigrants in the susceptible and infected classes. The panels in the top, middle, and bottom rows, respectively, give the timing to 10, 25, and 50% (percentiles) of measles cases. The panels in the left, middle, and right columns show results from the nighttime lights–informed model, the model with no migration, and the model with a constant level of migration, respectively. Within each panel, box plots indicate the distribution of the time (in days since the start of the observed epidemic, *x* axis) to the percentile of cases from 25,000 simulated trajectories for each commune (commune 1 in grey, commune 2 in red, commune 3 in green) for 5 ratios of susceptible to infected immigrants (from top to bottom, 100:1, 50:1, 25:1, 10:1, 1:1). Each box indicates the interquartile range (box) and median (central line); whiskers extend to the nearest point less than 1.5 times the interquartile range. Vertical lines indicate the observed timing of the percentile of cases for each commune (commune 1 in grey, commune 2 in red, commune 3 in green) from the 2003–04 outbreak. **Left column:** Under the nighttime lights–informed model, timing of the percentiles of cases were sensitive to the assumed ratio of susceptible to infected individuals. **Center column:** Only one box plot is shown for the model with no migration as the ratio of susceptible to infected immigrants is irrelevant when migration is set to 0. **Right column:** The constant migration model was insensitive to the ratio of susceptible to infected immigrants.

Table S1. For each city, columns indicate the following: approximate size (as measured by ~1-km image pixels), population size (as detailed above), difference between the maximum and minimum values of smoothed brightness for each city, the mean value of smoothed brightness for each city.

City	No. pixels	Population	Brightness range	Brightness mean
Niamey	340	828,734	1.38	24.38
Maradi	116	414,551	0.80	10.32
Zinder	117	344,271	0.79	12.56
Agadez	79	154,903	0.61	12.26
Katsina	273	318,459	2.43	16.81

.

Table S2. Estimated log-likelihood for each commune and model. Maximum log-likelihood for each commune is given in bold.

Model, commune	**Log likelihood**
Nighttime lights, commune 1	**–937**
No migration, commune 1	–1122
Constant migration, commune 1	–1020
Nighttime lights, commune 2	**–708**
No migration, commune 2	–842
Constant migration, commune 2	–746
Nighttime lights, commune 3	**–428**
No migration, commune 3	–466
Constant migration, commune 3	–495

Table S3. Parameter values (95% credible intervals given in brackets) for each commune and model; β = constant transmission parameter; Θ = slope of linear function of nighttime light-dependent migration rate.

Model, commune	**log(β)**	**log(Θ)**	**log(S_0)**
Nighttime lights, commune 1	–11.26 (–11.45, –10.99)	9.17 (8.35,9.88)	9.61 (9.38,9.88)
Nighttime lights, commune 2	–11.12 (–11.31, –10.36)	9.09 (8.14,10.16)	9.36 (9.06,9.65)
Nighttime lights, commune 3	–10.67 (–11.08,–10.30)	7.07 (0.89,10.69)	9.32 (8.49,10.02)
	log(β)	**log(Θ)**	**log(S_0)**
No migration, commune 1	–11.31 (–11.46, –11.04)	NA	9.88 (9.56,10.09)
No migration, commune 2	–11.29 (–11.46,–10.92)	NA	9.81 (9.41,10.06)
No migration, commune 3	–10.85 (–11.47,–10.23)	NA	9.17 (8.06,10.25)
	log(β)	**log(migration)**	**log(S_0)**
Constant migration, commune 1	–10.85 (–11.46, –10.24)	–2.51 (–7.75,2.68)	9.16 (8.06,10.25)
Constant migration, commune 2	–10.98 (–11.48,–10.31)	1.56 (–2.66,2.96)	9.08 (8.07,10.15)
Constant migration, commune 3	–10.84 (–11.46,–10.23)	0.09 (–6.63,2.86)	9.20 (8.11,10.22)

Table S4. For each commune, columns indicate the following: size of each commune (as measured by ~1 km image pixels), the mean value of smoothed brightness for each commune, difference between the maximum and minimum values of smoothed brightness for commune, and the total number of reported measles cases per commune during the 2003–2004 epidemic.

Commune	**No. pixels**	**Brightness mean**	**Brightness range**	**Total measles cases**
Commune 1	136	25.07	3.01	5934
Commune 2	153	25.01	1.63	4350
Commune 3	51	21.35	4.40	653

References

1. M. J. Ferrari *et al*., Rural-urban gradient in seasonal forcing of measles transmission in Niger. *Proc. Biol. Sci.* **277**, 2775 (2010). doi:10.1098/rspb.2010.0536 Medline

2. M. J. Ferrari *et al*., The dynamics of measles in sub-Saharan Africa. *Nature* **451**, 679 (2008). doi:10.1038/nature06509 Medline

3. W. P. London, J. A. Yorke, Recurrent outbreaks of measles, chickenpox and mumps. I. Seasonal variation in contact rates. *Am. J. Epidemiol.* **98**, 468 (1973).

4. D. P. Word, J. K. Young, D. A. T. Cummings, D. C. Laird, paper presented at the 20th European Symposium on Computer Aided Process Engineering— ESCAPE20, Ischia, Naples, Italy, 6 to 9 June 2010.

5. S. S. Hutchins *et al*., A school-based measles outbreak: The effect of a selective revaccination policy and risk factors for vaccine failure. *Am. J. Epidemiol.* **132**, 157 (1990). Medline

6. S. Altizer *et al*., Seasonality and the dynamics of infectious diseases. *Ecol. Lett.* **9**, 467 (2006). doi:10.1111/j.1461-0248.2005.00879.x Medline

7. N. C. Grassly, C. Fraser, Seasonal infectious disease epidemiology. *Proc. Biol. Sci.* **273**, 2541 (2006). doi:10.1098/rspb.2006.3604 Medline

8. R. M. Anderson, R. M. May, *Infectious Diseases of Humans: Dynamics and Control* (Oxford Univ. Press, New York, 1991).

9. M. Keeling, P. Rohani, *Modeling Infectious Diseases in Human and Animals* (Princeton Univ. Press, Princeton, NJ, 2008).

10. R. M. Prothero, Populations movements and tropical health. *Glob. Change Hum. Health* **3**, 20 (2002). doi:10.1023/A:1019636208598

11. J. L. Aron, I. B. Schwartz, Seasonality and period-doubling bifurcations in an epidemic model. *J. Theor. Biol.* **110**, 665 (1984). doi:10.1016/S0022-5193(84)80150-2 Medline

12. M. J. Keeling, B. T. Grenfell, Disease extinction and community size: Modeling the persistence of measles. *Science* **275**, 65 (1997). doi:10.1126/science.275.5296.65 Medline

13. R. H. Faulkingham, P. F. Thorbahn, Population dynamics and drought: A village in Niger. *Population Studies* **29**, 463 (1975). doi:10.2307/2173939 Medline

14. D. Rain, *Eaters of the Dry Season: Circular Labor Migration in the West African Sahel* (Westview Press, Boulder, CO, 1999).

15. C. D. Elvidge, K. E. Baugh, E. A. Kihn, H. W. Kroehl, E. R. Davis, Mapping city lights with nighttime data from the DMSP Operational Linescan System. *Photogramm. Eng. Remote Sensing* **63**, 734 (1997).

16. P. Sutton, D. Roberts, C. D. Elvidge, K. E. Baugh, Census from heaven: An estimate of the global human population using night-time satellite imagery. *Int. J. Remote Sens.* **22**, 3061 (2001). doi:10.1080/01431160010007015

17. J. Agnew, T. W. Gillespie, J. Gonzalez, B. Min, Baghdad nights: Evaluating the US military 'surge' using nighttime light signatures. *Environ. Plan. A* **40**, 2285 (2008). doi:10.1068/a41200

18. R. F. Grais *et al*., Estimating transmission intensity for a measles epidemic in Niamey, Niger: Lessons for intervention. *Trans. R. Soc. Trop. Med. Hyg.* **100**, 867 (2006). doi:10.1016/j.trstmh.2005.10.014 Medline

19. M. Begon *et al*., A clarification of transmission terms in host-microparasite models: Numbers, densities and areas. *Epidemiol. Infect.* **129**, 147 (2002). doi:10.1017/S0950268802007148 Medline

20. K. R. Yaméogo *et al*., Migration as a risk factor for measles after a mass vaccination campaign, Burkina Faso, 2002. *Int. J. Epidemiol.* **34**, 556 (2005). doi:10.1093/ije/dyi001 Medline

21. M. C. C. Camargo, J. C. de Moraes, V. A. U. F. Souza, M. R. Matos, C. S. Pannuti, Predictors related to the occurrence of a measles epidemic in the city of São Paulo in 1997. *Rev. Panam. Salud Publica* **7**, 359 (2000). doi:10.1590/S1020-49892000000600001 Medline

22. D. Balk *et al*., Determining Global population distribution: Methods, applications and data. *Adv. Parasitol.* **62**, 119 (2006). doi:10.1016/S0065-308X(05)62004-0

23. J. Dobson, E. Bright, P. R. Coleman, R. Durfee, B. Worley, LandScan: A global population database for estimating populations at risk. *Photogramm. Eng. Remote Sensing* **66**, 849 (2000).

24. M. C. González, C. A. Hidalgo, A. L. Barabási, Understanding individual human mobility patterns. *Nature* **453**, 779 (2008). doi:10.1038/nature06958 Medline

25. A. Noor, V. Alegana, P. Gething, A. Tatem, R. Snow, Using remotely sensed night-time light as a proxy for poverty in Africa. *Popul. Health Metr.* **6**, 5(2008). doi:10.1186/1478-7954-6-5

26. S. Ebener, C. Murray, A. Tandon, C. C. Elvidge, From wealth to health: modelling the distribution of income per capita at the sub-national level using night-time light imagery. *Int. J. Health Geogr.* **4**, 5 (2005). doi:10.1186/1476-072X-4-5 Medline

27. C. D. Elvidge *et al*., A global poverty map derived from satellite data. *Comput. Geosci.* **35**, 1652 (2009). doi:10.1016/j.cageo.2009.01.009

28. Niger Ministry of Health, Weekly measles case reports, 1995–2004 (Niger Ministry of Health, Niamey, 2008).

29. N. Bharti *et al*., Measles hotspots and epidemiological connectivity. *Epidemiol. Infect.* **138**, 1308 (2010). doi:10.1017/S0950268809991385 Medline

30. NOAA National Weather Service, Daily rainfall estimates, 2003–2006 (NOAA, 2009).

31. A. Tatem, A. Noor, S. Hay, Assessing the accuracy of satellite derived global and national urban maps in Kenya. *Remote Sens. Environ.* **96**, 87 (2005). doi:10.1016/j.rse.2005.02.001

32. C. D. Elvidge *et al*., A Fifteen Year Record of Global Natural Gas Flaring Derived from Satellite Data. *Energies* **2**, 595 (2009). doi:10.3390/en20300595

33. R Development Core Team, *R: A Language and Environment for Statistical Computing* (R Foundation for Statistical Computing, Vienna, Austria, 2008).

34. P. Sutton, D. Roberts, C. D. Elvidge, H. Meij, A comparison of nighttime satellite imagery and population density for the continental United States. *Photogramm. Eng. Remote Sensing* **63**, 1313 (1997).

35. C. Dubray *et al*., Late vaccination reinforcement during a measles epidemic in Niamey, Niger (2003-2004). *Vaccine* **24**, 3984 (2006). doi:10.1016/j.vaccine.2006.01.049 Medline

36. B. F. Finkenstädt, B. T. Grenfell, Time series modelling of childhood diseases: a dynamical systems approach. *J. R. Stat. Soc. Ser. C Appl. Stat.* **49**, 187 (2000). doi:10.1111/1467-9876.00187

37. H. J. Wearing, P. Rohani, M. J. Keeling, Appropriate models for the management of infectious diseases. *PLoS Med.* **2**, e174 (2005).

38. A. Doucet, N. De Freitas, N. Gordon, *Sequential Monte Carlo Methods in Practice* (Springer, New York, 2001).

39. O. N. Bjørnstad, B. Finkenstädt, B. T. Grenfell, Dynamics of measles epidemics: scaling noise, determinism, and predictability with the TSIR model. *Ecol. Monogr.* **72**, 185 (2002). doi:10.1890/0012-9615(2002)072[0185:DOMESN]2.0.CO;2

40. C. Viboud *et al*., Synchrony, waves, and spatial hierarchies in the spread of influenza. *Science* **312**, 447 (2006). doi:10.1126/science.1125237 Medline